Journal of Thermal Analysis and Calorimetry, Vol. 95 (2009) 1, 117–122

AN INVESTIGATION OF THE THERMAL DECOMPOSITION OF GOLD ACETATE

S. D. Bakrania[*], *G. K. Rathore and Margaret S. Wooldridge*

Department of Mechanical Engineering, University of Michigan, 2350 Hayward Street, Ann Arbor, MI 48109, USA

The thermal decomposition characteristics of gold acetate to produce gold nanoparticles were investigated. A rapid and violent fragmentation of the gold acetate particles was observed at approximately 103±20°C when a rapid heating rate of 25°C min^{-1} was used, leading to formation of nanosized spherical and partially coalesced gold particles. Particle size analysis was used to investigate possible relationships between the gold acetate crystallite size and the gold nanoparticles produced by thermal decomposition. The results indicate rapid (<0.14 ms) coalescence of the gold particles occurs for fragments in close proximity.

Keywords: *gold acetate, nanoparticles, thermal decomposition*

Introduction

Metal acetates are used as metal precursors in many nanoparticle synthesis methods, including oxidation [1], combustion [2, 3], anaerobic solution [4] and thermal precipitation synthesis methods [5], to name a few. The many recent advances in these and other synthesis methods have facilitated exploring broader applications of metal and metal oxide nanoparticles by utilizing the synthesis methods to augment the electrical, optical and chemical properties of the materials. The crystalline phase, degree of oxidation and particle morphology and size are strongly dependent on the synthesis process and, further, the reactant precursor used for the metal nanoparticles [6]. For example, earlier studies conducted in our laboratory have indicated there is a strong relationship between the decomposition properties of the solid phase metal acetate precursors and the product metal/metal oxide nanocomposite materials created during combustion synthesis [2]. However, there is little understanding of the fundamental physical and chemical mechanisms that govern the decomposition of metal acetates in these combustion and other synthesis systems which rely on thermal decomposition and oxidation of metal acetates [6].

Combustion synthesis has proved to be a versatile production technique for metal oxides and carbon-based particles such as silica (SiO_2), titania (TiO_2), alumina (Al_2O_3) and carbon black. Recent developments have expanded the scope of combustion synthesis to the generation of metal nanoparticles [7], nanocomposites [8] and one-dimensional structures [9] – focusing on the morphology and size, as much as the composition of the material itself. This renewed interest is attributed to new discoveries on functional nanomaterials for catalysis, electronics, medical imaging, drug targeting and sensing applications [10–12]. Combustion synthesis provides a direct production route to such revolutionary particles and the range of materials that can be produced using combustion synthesis has been dramatically increased by diversifying the precursor compounds to include solid-phase reactant precursors such as metal acetates [2, 13].

The current work focuses on identifying the mechanisms important during thermal decomposition of metal acetates in an oxidizing environment. The results of this study have relevance to combustion, pyrolysis and oxidation synthesis methods which use metal acetates as reactant precursors and to synthesis methods which use solid-phase organometallic precursors for generating nanoparticles [14, 15]. One of the major objectives of the investigation was to evaluate if there is a direct relationship between the average crystallite size of the metal acetate and the resulting metal nanoparticles produced. Gold acetate was selected for the study due to the importance of gold nanoparticles in many advanced optical, electrical and catalytic applications and the strong dependence of material performance on the size of the gold nanoparticles [16–19]. In particular, the experiments were designed to elucidate the early steps in the synthesis process, when metal acetate particle decomposition occurs. The initial steps in this process are critical in determining the characteristics of the final product nanoparticles.

Experimental

A combination of experimental strategies was employed to characterize the early stages of the gold acetate decomposition process. In one set of experiments, gold

* Author for correspondence: bakrania@rowan.edu

1388–6150/$20.00

Akadémiai Kiadó, Budapest, Hungary
Springer, Dordrecht, The Netherlands

acetate particles were heated on a hot-plate in air. High-speed imaging was used to capture the fragmentation of the metal acetate particles. Electron microscopy of unreacted and product particles ejected during decomposition was used to identify characteristic particle sizes and morphologies. X-ray diffraction (XRD) of the unreacted gold acetate was used to determine the average crystallite size of the powders. XRD spectra were also obtained for partially decomposed gold acetate to investigate changes in the reactant composition during the early stage of decomposition process. Because little is known regarding the thermal decomposition of gold acetate, another set of experiments using thermogravimetric analysis (TG) was used to confirm the general characteristics observed in the hot-plate studies.

All experiments were conducted using gold(III) acetate ($Au(C_2H_3O_2)_3$, Alfa Aesar, 99.96% Au). The as-received powders ranged in color from light brown to black. The source of the variability in the color (e.g. differences in particle size, partial decomposition of the powders, etc.) was not identified by the manufacturer. Based on the results of this study (presented and discussed below), the color change is likely due to partial decomposition of the gold acetate powders.

For the hot-plate experiments, the powders were heated at a rate of approximately 25°C min^{-1} (Fisher Scientific, Thermix Hot Plate Model 300T) in room air. This heating rate was selected because it was considered more representative of synthesis processing conditions for metal acetates than lower heating rates and lower heating rates did not yield physical fragmentation of the reactant particles. A high-speed digital imaging video camera (Vision Research, Phantom v.7.1, Nicor 50 mm lens f/0.95) was positioned approximately 100 mm from the hot plate for side-view imaging of the gold acetate particles. A 15 mm c-mount extension tube was used with the camera to optimize image quality. A metal halide lamp (ED 28 Universal bulb, 400W) was used to illuminate the decomposing particles on the hot plate.

The following procedure was used for the hot plate experiments. Gold acetate particles ranging from 0.5–1.0 mm in size were placed approximately 30 mm from the edge of the hot plate. The high-speed imaging camera was operated at 4800 frames per second (208 μs) with a spatial resolution of 800×600 pixels. The exposure time was set to 19 μs. The camera was manually triggered to record the particle decomposition process after particle heating was initiated. During the experiments, a K-type thermocouple was used to record the temperature of the hot plate approximately 2 mm away from the gold acetate particles.

Powders before and after the decomposition process were collected for analysis using electron microscopy. The as-received gold acetate powders were deposited on copper tape and sputter coated with Au–Pd (to improve image contrast) and then imaged using a scanning electron microscope (SEM, Philips XL30). The products of the heated gold acetate particles were collected by direct deposition of the particles ejected during decomposition onto transmission electron microscope (TEM) grids. The TEM grids (3 mm diameter, Electron Microscopy Sciences, carbon film, 300 mesh copper) were placed vertically at distances of 1, 2 and 4 mm away from the initially unreacted gold acetate particles. Samples of the ejected particles were obtained in order to monitor the evolution of the particles after fragmentation. The morphology of the decomposition products of the gold acetate were recorded using TEM imaging (Philips CM-12 Transmission Electron Microscope). Particle size information was determined from the TEM images using ImageJ, a Java-based image processing program [20]. For the image processing, the TEM files were converted to 8-bit grey-scale for auto-thresholding to separate the fragmented particles from the background of the images.

Unreacted (as-received) gold acetate powders and partially decomposed gold acetate powders were analyzed by XRD. Scans for phase identification and for average crystallite size of the unreacted powders were obtained using an automated Scintag Theta–Theta XRD with increments of 0.02° 2θ and CuK_α radiation (λ=1.5406 Å). The scans were obtained over a 2θ range of 5–70° at a scan rate of 1° 2θ min^{-1}. Spectral scans for average crystallite size were measured over a 2θ range of 11–16° at a scan rate of 0.5° 2θ min^{-1}. The average crystallite size was determined from the XRD spectra using the Scherrer equation,

$$d_{XRD} = \frac{0.9\lambda}{\beta_{1/2}\cos\theta}$$

where d_{XRD} is the average crystallite size, λ is the source wavelength, $\beta_{1/2}$ is the full width at half maximum of the peak used for the analysis and θ is the XRD scattering angle of the peak. The partially decomposed powders were obtained by heating the powders at 110°C for 1 h (prior to particle fragmentation, discussed above). The XRD scans of these materials were used to determine the degree of decomposition of the gold acetate and the relationship between reactant decomposition and the acetate color.

The TG experiments were conducted in an inert (nitrogen) environment using a heating rate of 5°C min^{-1} (TA Instruments Q50). Samples of approximately 4 mg of gold acetate powders were used. The metal acetate particles were not size-selected and were representative of the as-received powder. The gold acetate used in the TG study was darker in color than the powders used in the hot-plate experiments. As noted earlier,

the darker color indicated some partial decomposition of the reactant materials had occurred. This was not considered a concern for the TG experiments as the intention was to verify the decomposition temperature, which remained clearly identifiable in the TG time-histories.

Results and discussion

Characteristic particle size and morphology

Representative XRD patterns of the as-received gold acetate and heated sample are presented in Fig. 1. The JCPDS database does not have a reference pattern for gold acetate. Consequently, the XRD spectra for gold acetate reported by Kristl and Drofenik [21] is provided in the figure as a basis for comparison. As seen in the figure, the XRD pattern for the gold acetate used in this work is consistent with the previous XRD pattern for gold acetate documented in the literature; however, each spectra indicate some gold impurities (e.g. the features at 2θ=38.17 and 44.37°). The heated gold acetate spectra were used to determine if the gold impurity was from partial decomposition of gold acetate. The degree of decomposition can be assessed by evaluating the gold <111> peak intensity relative to the gold acetate peak intensity of the feature at approximately 2θ=14.5° for the as-received and heated gold acetate powders. A comparison of the difference in peak intensities normalized by the gold acetate peak height indicates greater presence of gold in the heated sample ($I_{\text{gold acetate}} - I_{\text{gold}}/I_{\text{gold acetate}}$=0.11) compared to the as-received powders ($I_{\text{gold acetate}} - I_{\text{gold}}/I_{\text{gold acetate}}$=0.43); suggesting greater degree of decomposition has occurred in the heated sample. This experiment also yielded a change in color from light brown (for the as-received powders) to dark brown (for the heated gold acetate powders). As a consequence, we concluded that the darker gold acetate powders are more partially decomposed than the light brown powders.

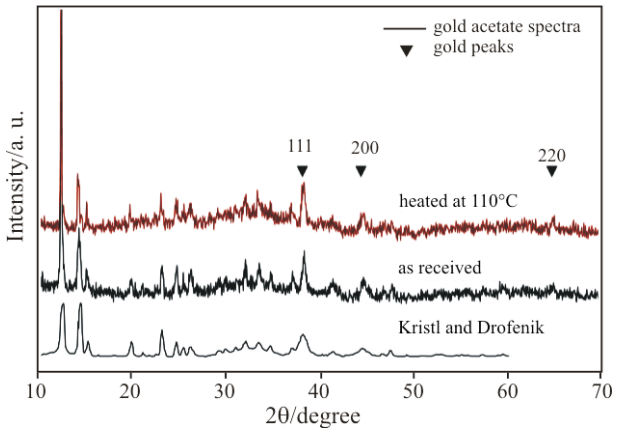

Fig. 1 Typical X-ray diffraction patterns of as-received (light brown in color) and heated (dark brown) gold acetate powders. A reference XRD pattern presented in Kristl and Drofenik [19] for gold acetate and the JCPDS reference for metallic gold are provided for comparison

Figure 2 shows SEM images of the as-received gold acetate powders. The images show the powders have a highly porous structure formed by finer grains that are less than 1 μm in size. XRD Scherrer analysis of the as-received light brown powders yielded an average crystallite size of 160 nm for the gold acetate used in this study.

Figure 3 presents a typical imaging sequence of the gold acetate decomposition and fragmentation process that occurred during each experiment. The first panel of Fig. 3 shows three gold acetate particles on the hot plate at the start of the experiment. The second panel shows the initial asymmetric fragmentation of the center gold acetate particle. A sharp cracking sound was also heard at this time. Figure 3c shows the formation of a nebula of particle fragments that occurred a fraction of a second (Δt=208 μs) after the first decomposition event. The decomposition temperature, defined as the temperature of the hot plate when the particles fragmented, was 103°C with an uncertainty of ±20°C (based on the standard deviation of multiple experiments). Although not apparent in the images in Fig. 3, the gold acetate particles also changed in color from light brown to dark brown/black before fragmentation was observed. After the experiments had concluded, pink streaks forming fairly uniform radial patterns of nanosized metallic gold were identified on the hot plate.

As noted earlier, samples of the particles ejected during decomposition were acquired at various locations near the hot plate by direct deposition onto

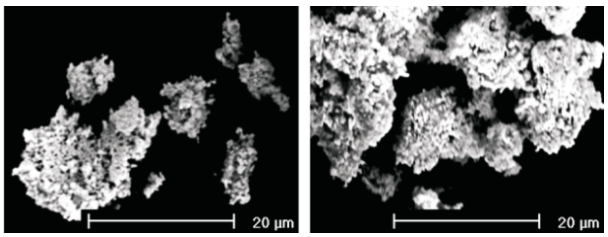

Fig. 2 SEM images of as-received gold acetate powder

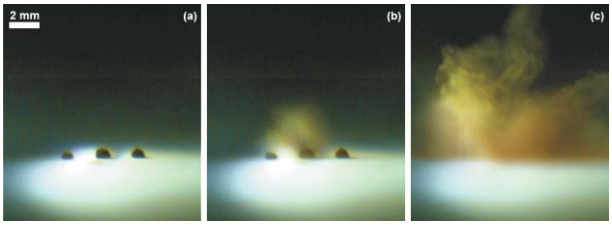

Fig. 3 Typical imaging sequence showing the progression of gold acetate particle decomposition and fragmentation after heating at 25°C min^{-1} was initiated at t=0 min: a – t=0 min, b – t=~4 min, c – t=4 min 0.2 ms

TEM grids. In order to estimate the residence time of the particles sampled, a radial particle ejection velocity was calculated from the high-speed imaging sequence based on the evolution of the particle plume relative to the center of the gold acetate particle. The average minimum initial particle ejection velocity was 14 m s^{-1}. This average ejection velocity yields a residence time of 0.14 ms for a grid located 2 mm from the center of the source particle.

TEM images of the particle fragments collected during decomposition revealed generally spherical nanoparticles dispersed non-uniformly on the grids. All the particles present on the grid were identified as metallic gold using X-ray energy dispersive spectroscopy (XEDS). A typical TEM image of particles sampled at 1 mm is provided in Fig. 4a. There were two categories of particles observed in the TEM imaging as seen in Fig. 4a: discrete spherical particles and more densely co-located particles which often appear partially coalesced (circled features). Figures 4b and c show examples of two such clusters captured from two separate grids located 1 mm from the initial gold acetate particles. Grid samples collected at 4 mm did not produce such cluster patterns. Instead much larger (with diameters ranging from 50 to 100 nm) and highly dispersed spherical gold particles were observed, such as shown in Fig. 4d. Fast sintering rates are clearly present in this system, as samples obtained at 4 mm were dominated almost exclusively by large coalesced particles.

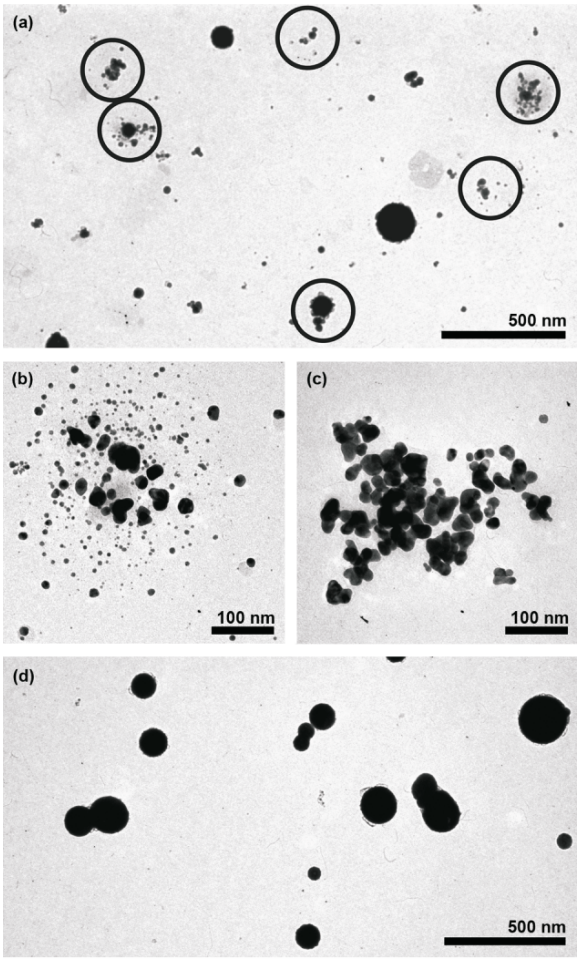

Fig. 4 TEM images of gold nanoparticles captured during gold acetate fragmentation. a – typical gold nanoparticles sampled at 1 mm; b, c – typical partially coalesced gold clusters sampled at 1 mm from two experiments; d – coalesced gold nanoparticles sampled at 4 mm

The TEM images were analyzed to determine the characteristic features of the gold fragment particles. In particular, the area of individual particles and cluster projected areas (defined as the total area of co-located and clustered fragmented particles) were measured from the images. The areas of the particles were used to determine the characteristic diameters of the discrete spherical particles, the diameters of the particles co-located within a cluster and the equivalent diameter that would be obtained if all the particles located in a cluster were coalesced. All image analysis assumed spherical particles. Analysis conducted on two grids sampled at 1 and 2 mm (obtained from two experiments) yielded coalesced sphere diameters of 140±65 and 171±54 nm, respectively. Here, the uncertainties represent the standard deviation in the particles analyzed. Individual particles in the clusters had diameters in the range of 5–10 nm. TEM images of the discrete spherical particles that were not part of the clusters yielded average diameters of 12.8±4.9 nm.

The TEM data can be compared to the characteristic dimensions of the unreacted gold acetate powders, where d_{XRD}=160 nm, to develop an understanding of the effects of the decomposition process on the gold nanoparticles produced. Our hypothesis, initially proposed in Bakrania *et al*. [2], is that the gold acetate crystallite grains are direct precursors to the initial gold particles formed and the crystallite grain dimensions therefore dictate the minimum dimension of the gold nanoparticles. The results of this work provide further data to consider this theory. Accounting for the molecular weight and density of gold acetate and gold, assuming complete conversion of gold acetate to metallic gold and assuming the gold acetate fragments along crystallite grains, the average crystallite size of 160 nm would yield spherical gold particles with an average diameter of 63 nm. This average is between the characteristic sizes determined for the larger coalesced particles (140±65 nm) and the smaller discrete particles (12.8±4.9 nm). While the results do not isolate a unique decomposition pathway, the results do point toward a relationship between the average crystallite size of the metal acetate reactant and the resulting metal nanoparticles.

Figure 5 presents a schematic of a decomposition mechanism based on the hypothesis described above

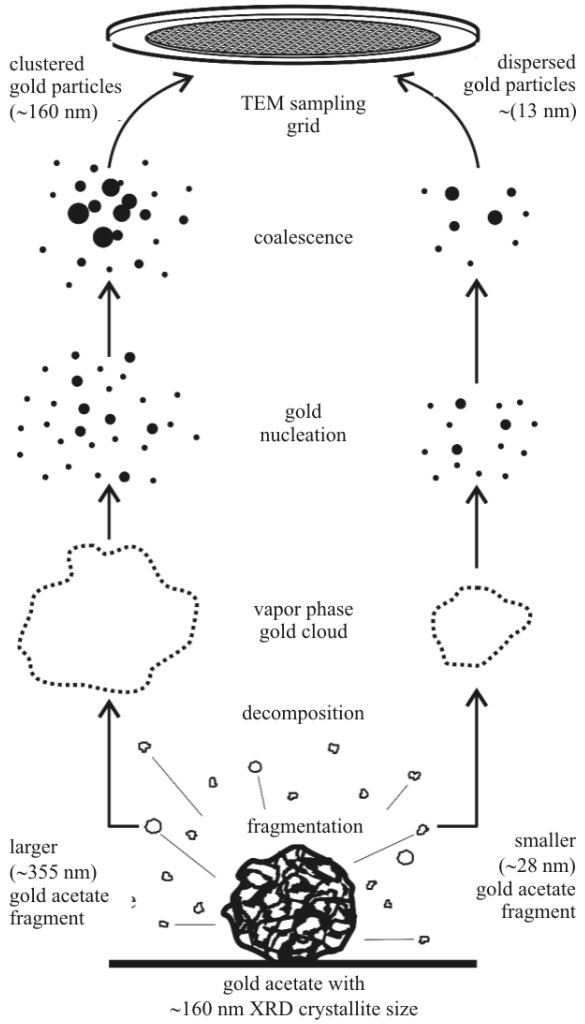

Fig. 5 Schematic of proposed gold acetate decomposition and gold particle formation mechanisms under rapid heating

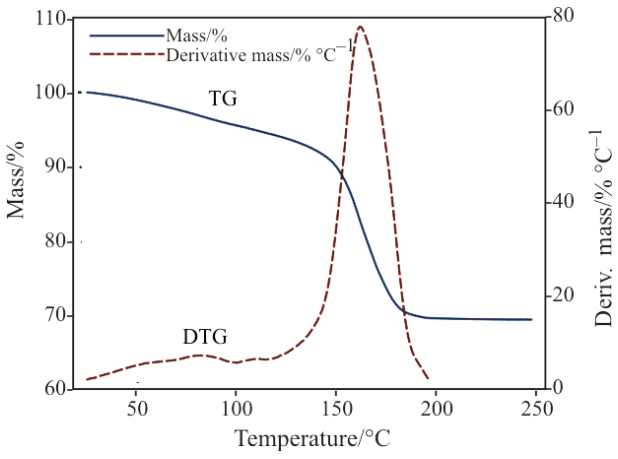

Fig. 6 TG curves for gold acetate in nitrogen using a heating rate of 5°C min^{-1}

and which is consistent with the experimental data observed in this study. Initially, heating causes discoloration of the particles indicating relatively slow gold acetate decomposition. This is rapidly followed by the explosive fragmentation stage, where fragments with a range of sizes (on the order of 160 nm) are ejected. The decomposition of metal acetates is typically highly exothermic [22–24]. These fragments can potentially be at much higher temperatures than the decomposition temperature of 100°C. The fragments form clouds of gold particles and vapor phase gold. Differences in the size of the clouds and the number density of gold affect the number of initial nucleation sites present within the cloud. Given similar residence times (~0.14 ms in the current study), higher number densities will yield more nucleation sites and higher interparticle collision frequencies than lower number densities. Consequently, more dense fragment clouds will yield more gold particles and larger gold particles (assuming rapid coalescence rates), such as shown in the reaction pathway on the left side of Fig. 5. Less dense clouds of particle fragments will form smaller and more discrete spherical particles, as shown in the reaction pathway on the right of Fig. 5. A range of initial particle fragment sizes is expected as the XRD data represent an average crystallite dimension. The rates of interparticle collision and coalescence dictate the final size of the gold nanoparticles.

Decomposition temperature

Figure 6 presents the thermogravimetric data for gold acetate mass loss under heating and the derivative of the percent mass loss with respect to temperature. Significant mass loss was observed between 120–210°C, with an average peak mass rate of loss occurring at T=170°C. Although the decomposition temperature measured during the hot plate experiments (103±20°C) was at a significantly different heating rate, the decomposition temperature is comparable to results obtained from the TG peak decomposition temperature.

The TG decomposition temperature for gold acetate agrees relatively well with other metal acetate thermal analysis such as palladium and copper acetate [22, 23, 25]. Such studies have suggested acetic acid is the dominant organic by-product when decomposition yields a pure metal. Note, the mass loss observed in these TG experiments was lower than expected; which is consistent with some partial decomposition of the powders prior to the analysis.

Conclusions

This work provides the first documentation of the dramatic particle fragmentation process that occurs

during heating of gold acetate in air. Measurements of the gold acetate decomposition temperature are in reasonable agreement and are consistent with expectations for metal acetates. The results of materials analysis supports that there is a relationship between the gold acetate crystallite size and the metal nanoparticles produced. Solid-phase metal-acetate precursors have tremendous potential to expand the composition and architecture of nanomaterials. This work provides key insights into the physical and chemical decomposition pathways that are important during decomposition of gold acetate and provides quantitative data that are critical for refining existing and developing new synthesis applications.

References

1 M. H. Khedr, A. A. Farghali and A. A. Abdel-Khalek, J. Anal. Appl. Pyrolysis., 78 (2007) 1.
2 S. D. Bakrania, T. A. Miller, C. Perez and M. S. Wooldridge, Combust. Flame, 148 (2007) 76.
3 T. A. Miller, S. D. Bakrania, C. Perez and M. S. Wooldridge, J. Mater. Sci., 20 (2005) 2977.
4 Z. Jia, S. Kang, D. E. Nikles and J. W. Harrell, IEEE Trans. Magnetics, 41 (2005) 3385.
5 M. Yin, Z. Chen, B. Deegan and S. O'Brien, J. Mater. Sci., 22 (2007) 1987.
6 M. Afzal, P. K. Butt and H. Ahmad, J. Thermal Anal., 37 (1991) 1015.
7 R. N. Grass and W. J. Stark, J. Nanoparticle Res., 8 (2006) 729.
8 A. Vital, A. Angermann, R. Dittmann, T. Graule and J. Töpfer, Acta Mater, 55 (2007) 1955.
9 R. L. Vander Wal, L. J. Hall and G. M. Berger, J. Phys. Chem. B, 106 (2002) 13122.
10 T. A. Miller, S. D. Bakrania, C. Perez and M. S. Wooldridge, Functional Nanomaterials, (2006).
11 O. V. Salata, J. Nanobi., 2 (2004) 3.
12 B. Delmon, J. Therm. Anal. Cal., 90 (2007) 49.
13 S. D. Bakrania, C. Perez and M. S. Wooldridge, Process Combust. Inst., 31 (2007) 1797.
14 D. Wostek-Wojciechowska, J. K. Jeszka, P. Uznanski, C. Amiens, B. Chaudret and P. Lecante, Mater. Sci.-Poland, 22 (2004) 407.
15 B. E. Hamaoui, L. Zhi, J. Wu, J. Li, N. T. Lucas, Ž. Tomović, U. Kolb and K. Müllen, Adv. Funct. Mater., 17 (2007) 1179.
16 M.-S. Hu, H.-L. Chen, C.-H. Shen, L.-S. Hong, B.-R. Huang, K.-H. Chen and L.-C. Chen, Nature Mater., 5 (2006) 102.
17 V. K. Pustovalov and V. A. Babenko, Laser Phys. Lett., 1 (2004) 516.
18 L. Pasquato, P. Pengo and P. Scrimin, J. Mater. Chem., 14 (2004) 3481.
19 M. Haruta, Nature, 437 (2005) 1098.
20 M. D. Abramoff, P. J. Magelhaes and S. J. Ram, Biophot. Intl., 11 (2004) 36.
21 M. Kristl and M. Drofenik, Inorg. Chem. Commun., 6 (2003) 1419.
22 P. K. Ghallagher and M. E. Gross, J. Thermal Anal., 31 (1986) 1231.
23 A. Obaid, A. Alyoubi, A. Samarkandy, S. Al-Thabaiti, S. Al-Juaid, A. El-Bellihi and El-H Deifallah, J. Therm. Anal. Cal., 61 (2000) 985.
24 R. M. Mahfouz, S. M. Alshehri, M. A. S. Monshi and N. M. Abd el-Salam, Radiat. Effects. Defects Solids, 159 (2004) 345.
25 J. Y. Zhang and I. W. Boyd, Appl. Phys. A: Mater. Sci. Proc., 65 (1997) 379.

Received: April 11, 2008
Accepted: August 12, 2008
OnlineFirst: November 12, 2008

DOI: 10.1007/s10973-008-9173-1